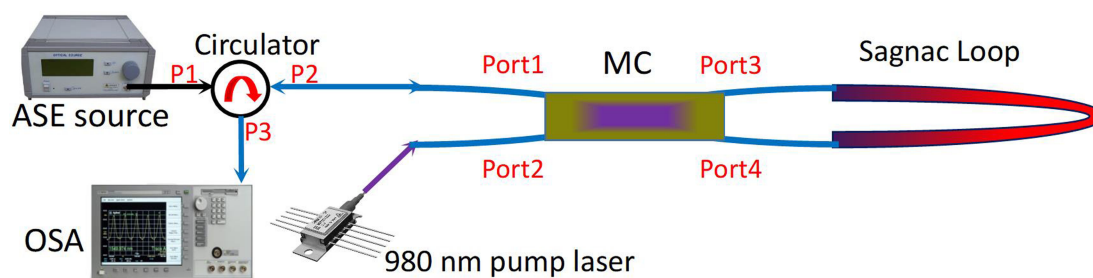


All-Optical Modulation Characteristics of a Microfiber Coupler Combined Sagnac Loop

Volume 11, Number 1, February 2019

Yang Yu
Qiang Bian
Jianfei Wang
Xueliang Zhang
Junbo Yang
Linmei Liang



DOI: 10.1109/JPHOT.2018.2886564
1943-0655 © 2018 IEEE

All-Optical Modulation Characteristics of a Microfiber Coupler Combined Sagnac Loop

Yang Yu ^{1,2}, Qiang Bian,² Jianfei Wang,² Xueliang Zhang,² Junbo Yang,¹ and Linmei Liang¹

¹College of Liberal Arts and Sciences, National University of Defense Technology, Changsha 410073, China

²College of Meteorology and Oceanology, National University of Defense Technology, Changsha 410073, China

DOI:10.1109/JPHOT.2018.2886564

1943-0655 © 2018 IEEE. Translations and content mining are permitted for academic research only.

Personal use is also permitted, but republication/redistribution requires IEEE permission.

See http://www.ieee.org/publications_standards/publications/rights/index.html for more information.

Manuscript received October 22, 2018; revised December 4, 2018; accepted December 10, 2018. Date of publication December 13, 2018; date of current version January 1, 2019. This work was supported by the National Natural Science Foundation of China under Grant 61805278. Corresponding author: Jianfei Wang (e-mail: wangjianfei09@nudt.edu.cn).

Abstract: In this paper, we theoretically and experimentally investigate the all-optical modulation characteristics of a microfiber coupler combined Sagnac loop (MCSL). We inject pump lights with different intensities into the MCSL and utilize the thermo-optical effect from the microfiber coupler to control the phase relationship between the counter-propagating beams inside the Sagnac loop. The spectral characteristics from the Sagnac loop can be controlled accordingly, and the rate of the frequency comb (interference characteristic wavelength) shift can be 1 pm/mW. In addition, at a specific wavelength (e.g., 1550 nm), the MCSL can be used as an intensity modulator as well as a reflectivity-tunable Sagnac reflector. The reflectivity variation of the Sagnac reflector can reach about 10% when the pump light is at milliwatt level. The intensity modulation depth can be 9.3% at 100 Hz when the intensity-modulated 980 nm pump light imposed on the MCSL is 5.5 mW. Based on the thermo-optical effect, the MCSL can achieve the all-optical intensity modulation and all optically tunable filtering functions. The device is expected to play an important role in the development of tunable, multi-wavelength, and compact fiber lasers.

Index Terms: Optical microfiber coupler, all-optical modulation, thermo-optic effect, tunable filter, intensity modulation.

1. Introduction

Fiber laser is one of the most important laser sources, which has been widely used in many fields, e.g., optical fiber communication network, optic sensing systems, atom clock and quantum computing etc. [1], [2]. In order to meet the requirements of large-scale distributed projects, environment monitoring and biosensing, fiber lasers with multi-wavelengths, tunability, low cost and high-performance optical interconnects are needed [3]–[6]. Several techniques have been proposed to realize tunable or multi-wavelength fiber lasers, including the distributed feedback Bragg lasers [7]–[9], the Rayleigh backscattering based ultra-narrowed linewidth fiber lasers [10], [11], modulation-instability-assisted four-wave mixing tunable fiber laser [12], time-dispersion-tuned technique [13], [14] etc. All of the above technologies could be regarded as inserting some types of fiber filters or modulators into the resonator to realize tunability or multiwavelength output [15]–[18].

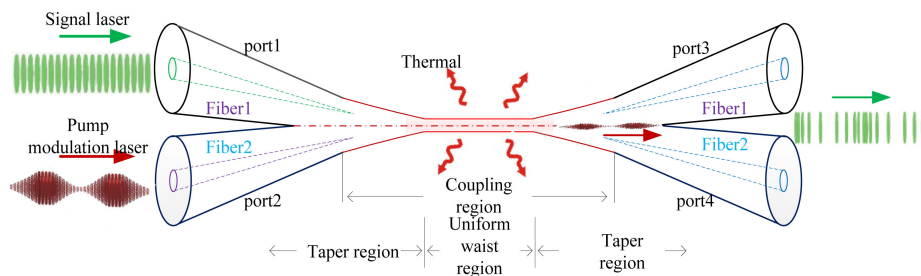


Fig. 1. Schematic diagram of the MC.

In addition, the tunable fiber filters and intensity modulators have been commonly used in wavelength/intensity modulation, Q-switch, mode selection in fiber lasers, and also in application fields such as sensing, microwave photonics and communication systems [19]–[22]. However, most of the existing tunable filters and modulators are realized generally based on electro-optic effects, thermo-optic effects, or elastic-optic effects and driven with electrical signal. They are too big or too complex for optical system integration and particularly, difficult to meet the application requirements for compact fiber laser development. Therefore, the development of new all-optical tunable filters, modulators and other functional devices is of great significance for the development of tunable fiber laser technology.

Owing to the advantages of easy integration with existing optical systems and high sensitivity to external environmental changes, microfiber couplers (MCs), especially fused and tapered by conventional fiber, have been widely used in sensing fields and fiber lasers [23]–[29]. And, as a novel fiber filter (the MC's filter characteristics are mainly determined by the coupling length and refractive index of the coupling region [30]), MCs could be used to adjust the characteristics of the fiber lasers. For example, a wavelength tunable Q-switched fiber laser has been realized by applying stress on the inner-cavity's MC [30]. A stable dual-output C-band multiwavelength fiber laser has been achieved based on features of the MC's spatial mode coupling and multi-transmission ports [29]. In addition, MC also shows potential to realize a single wavelength fiber laser by a special design to achieve a free spectral range (FSR) larger than the bandwidth of gain medium [30]. Compared with the traditional filters, MC based fiber filters possess advantages of easy fabrication, low cost, compact configuration, multi-transmission ports, and especially the ability of flexible structure design to realize different filter functions. However, the application of MCs as all-optical tunable components have not been reported. We have previously demonstrated that, the MC's all-optical intensity modulation could be realized based on the thermo-optic effect [31]. In addition, recent studies have shown that the MC combined Sagnac loop (MCSL) can achieve magnetic field, refractive index (RI) and twist sensing [23]–[27]. Especially, the Sagnac loop can be easily integrated into a fiber laser cavity as a reflection device, and can realize external cavity Q-switching, filtering and laser output functions [13]. In view of this, this paper integrates MC and Sagnac loop, and then conducts all-optical control research based on thermo-optic effect, in order to obtain functional devices such as all-optical tunable filters and intensity modulators that meet the development requirements of compact tunable fiber lasers.

2. Mechanism Analysis of the MCSL's All-Optical Control

In this paper, the MCSL is fabricated through connecting the Port 3 and Port 4 of the MC together, and the MC is fabricated by two twisted conventional fiber based on the improved flame-brushing method [29], [31]. The MC sample is comprised of taper region and uniform waist region, and the schematic diagram of the composition MC is shown in Fig. 1.

The total coupling of the MC composes of two parts: the transition region coupling and the uniform waist region coupling. Considering the coupling region changes slowly, local coupled mode theory

can be utilized to analyze the coupling property of MC [29], and the coupled power of the MC' two output ports (port 3, port 4) can be expressed as [23]–[29]:

$$\begin{cases} P_3 = P_0 \cos^2 \left(\int_0^l c(\lambda, n_2, z) dz \right) = P_0 \cos^2 \varphi \\ P_4 = P_0 \sin^2 \left(\int_0^l c(\lambda, n_2, z) dz \right) = P_0 \sin^2 \varphi \end{cases} \quad (1)$$

where P_0 is the input light power, l is the coupling length, $c(\lambda, n_2, z)$ is the coupling coefficient at wavelength λ and location z , n_2 is the cladding refractive index of the fiber. The thinner transition region and the uniform waist region of the MC plays an important role on mode coupling which can affect the coupling coefficient and also the output interferometric spectrum of the MC [29]. Then considering the stronger thermo-optic effect of the thinner waist region, so only the strong coupling region should be considered of the MC. For strong coupling case, the corresponding coupling coefficient is given by [29]–[31]:

$$c(\lambda, n_2, z) = \frac{3\pi\lambda}{32n_2r^2} \frac{1}{(1 + 1/V)^2} \quad (2)$$

where $V = [(2\pi r)/\lambda](n_2^2 - n_3^2)^{1/2}$ is the normalized frequency, r is the radius of the microfiber at the waist region, λ is the incident light wavelength, n_2 and n_3 are the refractive index of the fiber cladding and the external environment respectively.

As can be seen from reference [23], the cavity length of the Sagnac ring affects the MCSL's filtering characteristics. However, the Sagnac ring used in this paper is made of conventional single-mode fiber, and the birefringence effect is relatively limited. Therefore, when the cavity length of the Sagnac ring is not very large, the influence of the structural parameters of the Sagnac ring on the filtering characteristics of the MCSL can be ignored. For the MCSL, the lights from Port 3 and Port 4 propagate inside the Sagnac loop in the opposite directions to Port 4 and Port 3 respectively. After the MC coupling, the output light powers of MCSL's Port 1 and Port 2 can be expressed as [23]–[26]

$$P_1 = P_3 \sin^2 \varphi + P_4 \cos^2 \varphi = P_0 \frac{1}{2} \sin^2 (2\varphi) \quad (3)$$

$$P_2 = P_3 \cos^2 \varphi + P_4 \sin^2 \varphi = P_0 \left[1 - \frac{1}{2} \sin^2 (2\varphi) \right] \quad (4)$$

According to Eqs. (1)–(4), the light transmission characteristics of the MCSL are decided by the cladding refractive index n_2 , environmental refractive index n_3 , incident light wavelength λ , coupling length l and radius of microfiber at the waist region r . For a ready-made device in a stable environment, the light transmission characteristics mainly depend on n_2 and λ . Therefore, the output power P_2 varies with the light wavelength, and these relative variations can be detected by the optical spectrum analyzer (OSA). In addition, the corresponding interference characteristic wavelength will shift as n_2 changes.

As is shown in Fig. 1, by injecting an intensity-modulated pump light into MC from port 2, the partial pump light will be absorbed by the waveguide material, of which the energy converts to heat the waist region of the MC [31]. Owing to thermo-optical effect, the cladding refractive index n_2 will change, and the refractive index variation of the waveguide material Δn_2 can be written as

$$\Delta n_2 = \gamma \Delta T = \gamma \frac{\eta \alpha I_p}{C \rho \pi r^2} \quad (5)$$

Where γ is thermo-optic coefficient, ΔT is the temperature rise, η is the thermal conversion coefficient of the absorbed pump power, α is the loss coefficient for the pump light in the waist region, I_p is the intensity of pump light, C and ρ are the heat capacity and density of the waveguide material. According to Eqs. [1]–[5], the thermo-optic effect will induce the corresponding interference characteristic wavelength shift, and the spectral from the MCSL can be changed accordingly. The

wavelength shift caused by the refractive index change can be expressed as [24]

$$\Delta\lambda = \frac{\partial\lambda}{\partial n_2} \cdot \Delta n_2 = -\frac{\partial(2\varphi)/\partial n_2}{\partial(2\varphi)/\partial\lambda} \cdot \Delta n_2 \quad (6)$$

According to Eqs. (1)–(6), it is easy to obtain that $\partial\varphi/\partial n_2 < 0$, $\partial\varphi/\partial\lambda > 0$. Thus, if strong coupling dominates the whole coupling process of the MC, $\partial\lambda/\partial n_2 > 0$ and the dip wavelength will red-shift with the intensity of pump light increase.

In summary, by injecting pump lights with different intensities into the MCSL, the thermo-optical effect from the microfiber coupler will control the phase relationship between the counter-propagating beams inside the Sagnac loop. And the spectral characteristics from the Sagnac loop can be controlled accordingly. In addition, at a fixed operating wavelength, the intensity modulation can be achieved by utilizing the thermo-optic effect. Under the power modulation of the pump light, the power variations of Port 1 and Port 2 can be expressed as [25], [31]

$$\Delta P_1 = -\frac{P_0}{2} \sin^2 \left(2 \frac{\partial\varphi}{\partial n_2} \cdot \Delta n_2 \right) \quad (7)$$

$$\Delta P_2 = \frac{P_0}{2} \sin^2 \left(2 \frac{\partial\varphi}{\partial n_2} \cdot \Delta n_2 \right) \quad (8)$$

According to Eqs. [5]–[8], the output power of Port 1 will decrease and that of Port 2 will increase under the modulation of the pump light. The modulation efficiency is proportional to α , η , and l_p , and inversely proportional to r .

As can be seen from reference [23], the cavity length of the Sagnac ring affects the MCSL's filtering characteristics. However, the Sagnac ring used in this paper is made of conventional single-mode fiber, and the birefringence effect is relatively limited. Therefore, when the cavity length of the Sagnac ring is not very large, the influence of the structural parameters of the Sagnac ring on the filtering characteristics of the MCSL can be ignored. In addition, compared with MC and optical micrifer (OM), conventional fiber has lower light absorption and heat efficiency [31]. Therefore, the all-optical modulation and filtering characteristics of the MCSL are mainly determined by the structural parameters and thermo-optic characteristics of the MC.

3. Experiment and Discussion

The MC sample used for the MCSL in this paper is fabricated by fusing and tapering two twisted conventional communication fibers based on the improved flame-brushing method [31], [32], and with the length of the uniform waist region as 10 mm, and the radius of the microfiber as 0.9 μm . Figure 2(a) is the measured spectral characteristics of the MCSL and the MC sample's port3 by optical spectrum analyzer (OSA), with a spectral resolution of 0.01 nm. It can be seen from the spectral local test results that (as shown in Fig. 2(b)), the FSR of the MCSL is about 0.5 nm (which is half of the MC), and the bandwidth of the resonant wavelength is about 0.15 nm (FWHM). By optimizing the design of coupling region length and waist region diameter of the MC, the FSR and FWHM of the MCSL can be changed flexibly. Compared with the MC, the spectral of the MCSL distribution presents a characteristic as a dense comb filter, which demonstrates potential application value in the development of narrow spectral linewidth and multi-wavelength fiber laser.

3.1 Filter Control Experiment

In order to study the all-optical control characteristics of the MCSL transmission spectrum, the experimental setup shown in Fig. 3 was constructed. During the experiment, the 980 nm light source is connected to the port 2 of the MC, and then pump light with different intensity is injected into the MCSL to heat the MC's waist region. An amplified spontaneous emission (ASE) light source is used, and Inject light into the MCSL through a circulator (as shown in Fig. 3, the ASE is connected to the injected port (P1) of the circulator). The light from the straight port (P2) of the circulator is

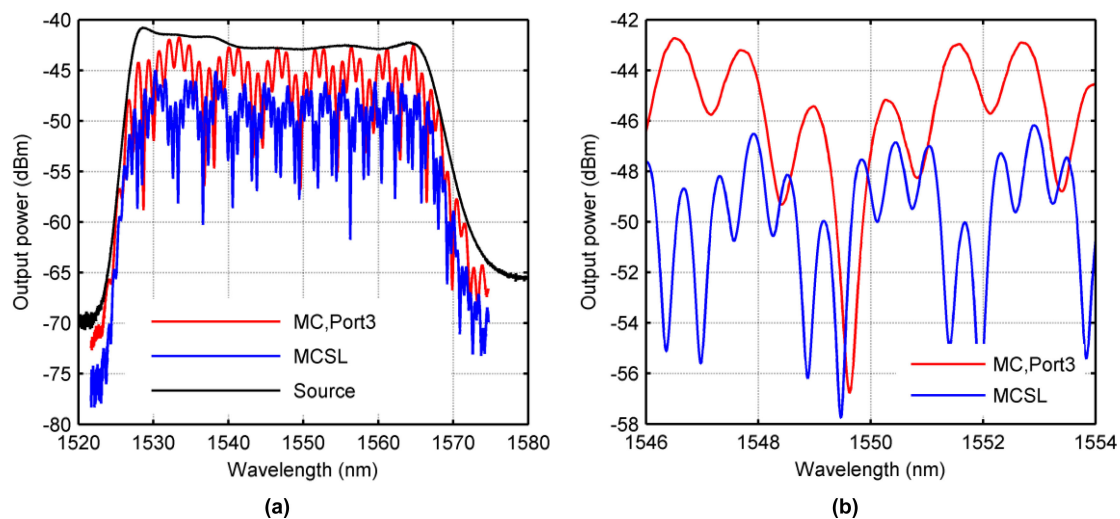


Fig. 2. (a) The transmission spectra of the MC and MCSL. (b) Partial test result magnified view.

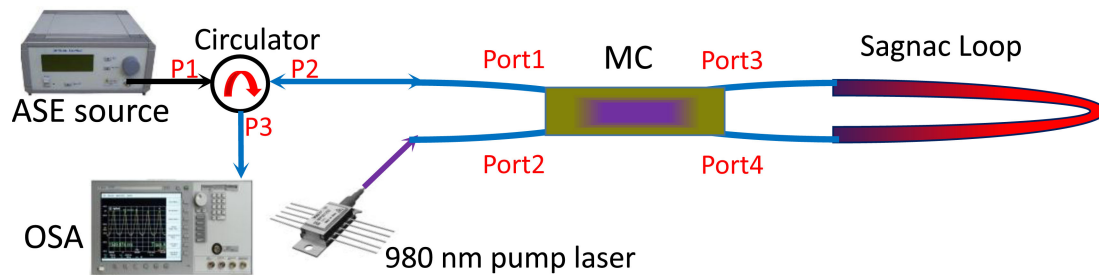


Fig. 3. Schematic of the experimental setup for MCSL's filter control experiment.

connected to Port 1 of the MC, reflected by the MCSL, then comes out from the reflective port (P3) of the circulator. The transmission characteristics of the MCSL is monitored by the OSA, and the transmission spectra of the MCSL under different pump powers is shown in Fig. 4.

As the results show that, with the increase of the injected pump power, the whole spectra (1520–1580 nm) red-shift. In the short-wave region, the spectral shift is large, that is, the adjustment efficiency is higher. Partial test result magnified view is shown in Fig. 4(b), which shows that under the action of different intensity pump light, the dip wavelengths of the two “interference characteristic wavelength” will shift, and at the same time, the intensity extreme values will also change.

The relation between the two interference characteristic wavelength shift and pump power (dip 1 1554.4 nm, dip 2 1556.3 nm when pump power is zero) is shown in Fig. 5(a). The two wavelength dips show nearly the same shift (~ 1 pm/mW) as the pump light increases. The results show that the spectral characteristics of the MCSL can be controlled under the action of all-optical control based on the thermo-optic effect. And the MCSL shows good all-optical tunable filter characteristics, and it is expected to be developed into all-optical, wideband and tunable filters after further optimization.

As is shown in Fig. 5(b), with the increase of pump light, the intensity extreme value corresponding to the interference characteristic wavelength dips will change. The rate of intensity change at dip 1 is -0.08 dB/mW and that at dip 2 is 0.05 dB/mW. It can be seen that, the MCSL can be used as a reflectivity Sagnac-tunable reflector and intensity modulator at a specific operating wavelength. At the same time, the MCSL output transmission intensity is different at different working wavelengths. Therefore, integrating MCSL into the cavity of a fiber laser is expected to achieve laser tunable intensity output and Q-switching.

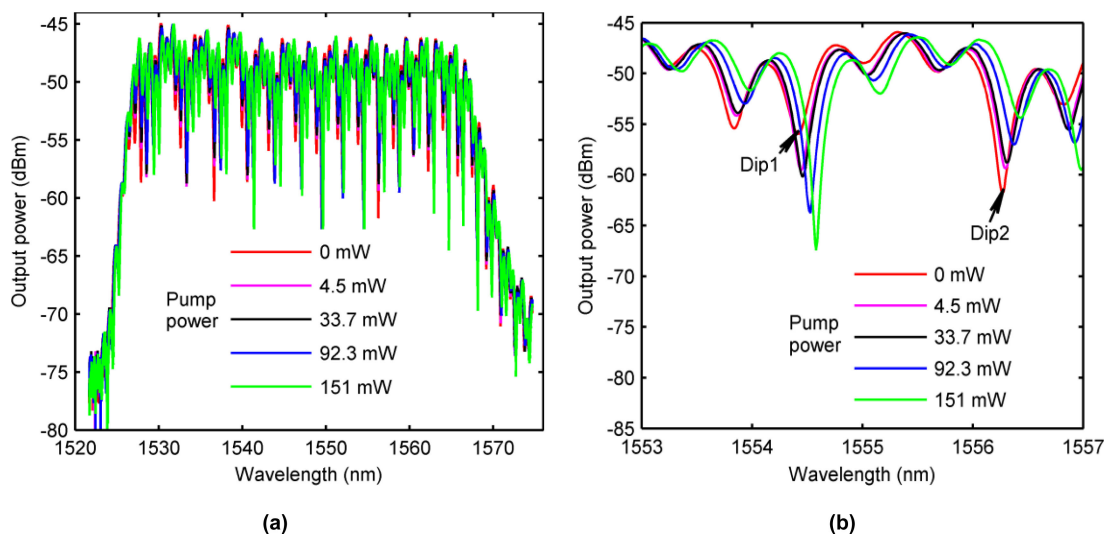


Fig. 4. (a) The transmission spectra of the MCSL under different pump power. (b) Partial test result magnified view.

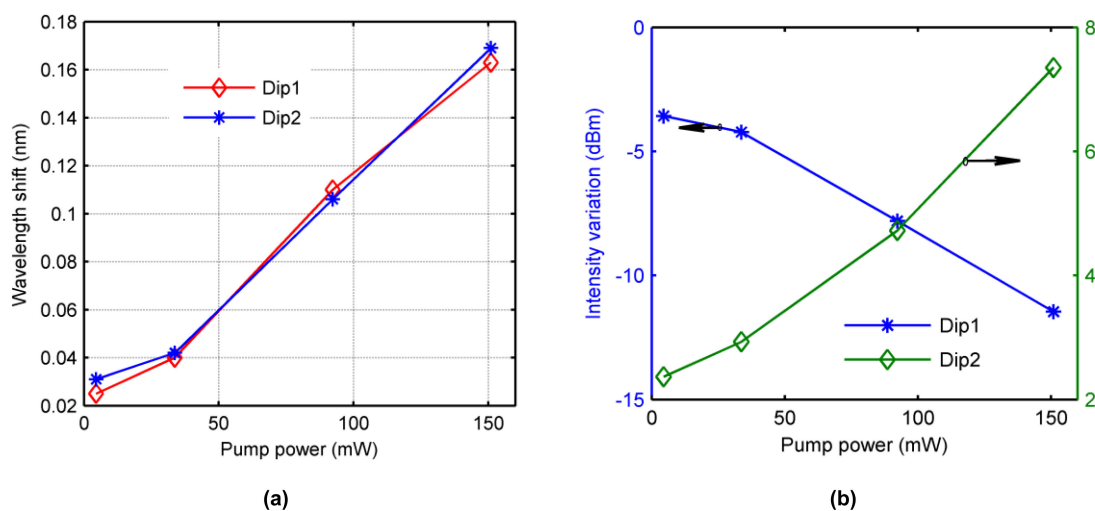


Fig. 5. (a) The wavelength shift of MCSL with different pump power. (b) The intensity variation of MCSL with different pump power.

The sample used in this paper only preliminarily verified the all-optical filtering control function of the MCSL, and the MC sample used were not optimized. In fact, the FSR of MC depends on the RI of waveguide material, the radius and length of the waist region. The FSR can be increased by reducing the MC uniform waist length, and reducing the MC waist diameter can effectively increase the modulation depth (ie, increase the wavelength shift). It means that, by improving the structural parameters of MC, different filter properties of MCSL can be achieved. For example, by increasing the radius of MC's waist region, the FSR of MC can be larger than the gain bandwidth of fiber laser's gain medium so the single wavelength output of fiber laser can be achieved [29], [30]. Similarly, the fiber laser can output multi-wavelength light if the FSR is smaller than the gain bandwidth of the gain medium [29]. Therefore, by improving the structural parameters, MCSL is expected to realize the capability of broadband and multi-band tunable filtering. In addition, according to the research experience based on MC intensity modulators, in order to achieve higher modulation efficiency and

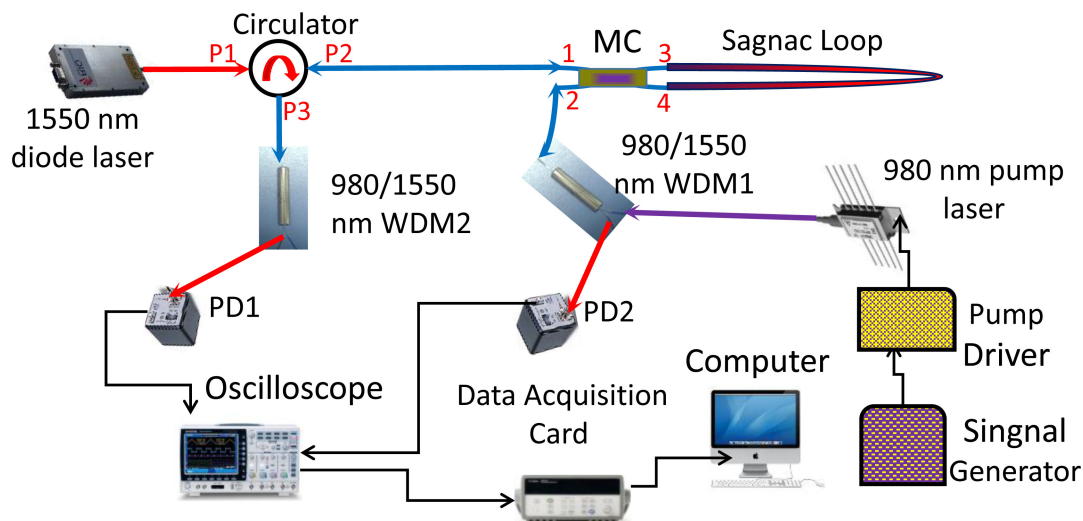


Fig. 6. Schematic of the experimental setup for MCSL's intensity modulation experiment.

faster modulation rate, the diameter of the waist region should be smaller than $8\ \mu\text{m}$ [31]. On the whole, the development of all-optical and wide-spectrum tunable filters based on the MCSL has certain optimization potentials, but further work is needed to meet the requirements of high-quality filter applications. For example, the MC waist-wound microcavity and the MC waist region can be covered with two-dimensional materials to further improve control performance of MC-based filters.

3.2 Intensity Modulation Experiment

The filter is the key to achieving laser wavelength selective output and tuning. However, in order to meet practical applications, tunable lasers must not only have the ability to control the output wavelength, but also have the ability to tune the output intensity. Therefore, the filter, if it has the intensity modulation capability, will have a better application prospect, especially in the development of tunable lasers. To investigate the intensity modulation characteristics of the MCSL, a 1550 nm diode laser with a bandwidth of 3 kHz was used as a probe light source. As shown in Fig. 6, the 1550 nm laser is injected into the MCSL through a circulator, passes through the MCSL, and then comes out from both Port 1 (to the circulator) and Port 2 (to the WDM1). An intensity-modulated 980 nm pump light is injected into the MCSL to heat the waist region of the MC. And the 980 nm diode laser is controlled by a pump driver (ILX Light wave LDC-37488B), the intensity modulation is realized by using an arbitrary waveform generator (AWG). The modulated 980 nm pump light first passes a 980/1550 nm wavelength division multiplexing (WDM1), and then enters into Port 2 of the MCSL, and the modulation characteristics can be investigated by monitoring output variations of the probe light at Port 1 and Port 2. The reflective port of the circulator is connected to another 980/1550 nm wavelength division multiplexing (WDM2), and the 1550 nm output port of this WDM1 is connected to the photodiode 1 for detection. The 1550 nm light from Port 2 of the MC enters into WDM1, and then is detected by photodiode 2. The signals from the photodiodes are recorded by an oscilloscope. The data is then dealt by a LabVIEW controlled data acquisition card and a computer.

Firstly, by applying low frequency triangle-wave signals with different amplitudes through AWG, the 980 nm pump light with different intensities were injected into the MCSL and the probe light output results of Port 1 and Port 2 are shown in Fig. 7. As is shown in Fig. 7, as the intensity of the 980 nm pump light increases, the output of Port 1 and Port 2 fluctuates in sync and the fluctuation range increases accordingly. In addition, the output intensity of Port 1 decreases synchronously with the increase of the output intensity of Port 2, which is consistent with the above theoretical analysis.

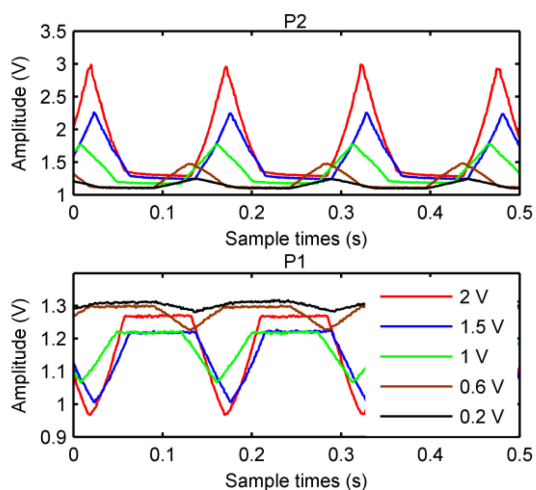


Fig. 7. The output results of Port 1 and Port 2 with different light intensity injected.

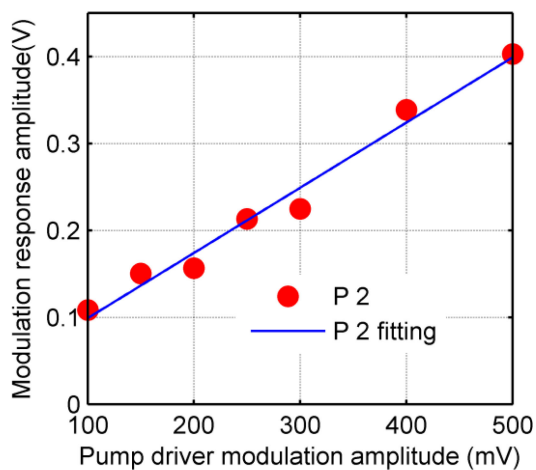


Fig. 8. The intensity modulation response characteristics with different modulation amplitudes.

Based on this result, a sine wave modulation signal having a fixed frequency of 100 Hz was applied to the 980 nm pump laser. The 980 nm pump laser outputs a standard sinusoidal intensity modulated signal with adjustable amplitude and frequency (modulation depth $M \approx 1$), and the average output optical power increases linearly with the pump driver modulation amplitude (output efficiency reaches $11 \mu\text{W}/\text{mV}$). Then the Port 1 and Port 2 output the sin wave modulation signals with the same frequency as the modulation signal. Figure 8 is the intensity response characteristics of MCSL's port2 with different 980 pump driver modulation amplitudes. As is shown in Fig. 8, when the modulation amplitude increases from 100 mV to 500 mV (1.1 mW to 5.5 mW), the modulation response amplitude of Port 2 increases dramatically (the modulation depth increasing from 7.3% to 9.3%). Consequently, at a specific wavelength, MCSL can be used as an intensity modulator as well as a tunable-reflectivity Sagnac reflector. And the reflector can achieve the reflectivity variation of about 10% when the pump light is at milliwatt degree.

Finally, the frequency response characteristics of MCSL's intensity modulation are investigated by fixing the 980 nm pump driver modulation amplitude at 200 mV and changing the modulation frequency from 0.2–40 kHz. The probe light intensity-modulated output signals at time domain

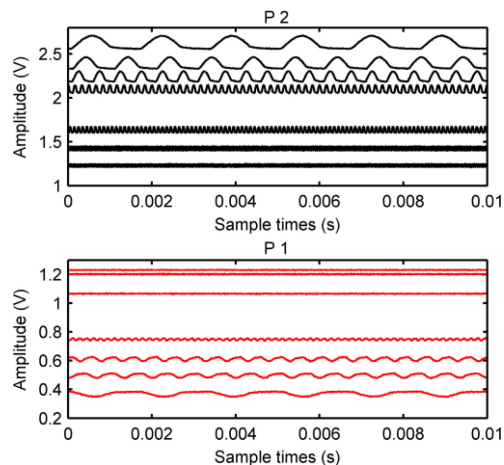


Fig. 9. The intensity-modulated output signals at time domain of Port 1 and Port 2.

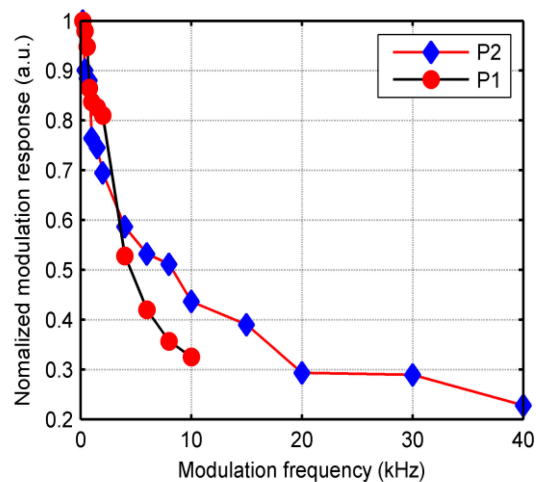


Fig. 10. The normalized amplitude-frequency results of Port 1 and Port 2.

of Port 1 and Port 2 are shown in Fig. 9. The modulation response amplitude of output signal decreases with the increase of modulation frequency.

The normalized amplitude-frequency results of these two output port are shown in Fig. 10. In order to eliminate the influence of system noise, 200 Hz was used as the benchmark in the normalization process. According to the test results, the normalized modulation response (modulation efficiency) is directly proportional to the modulation frequency. Referring to the test results of the all-optical modulation response of the MC, the frequency response characteristics of MCSL under intensity modulation mainly depend on the waveguide structure of MC's waist region and thermal conductivity [31], [32]. Therefore, the structure of MC's waist region can be improved to promote the intensity modulation efficiency of MCSL. Reference [31] introduced an MC-based intensity modulator that implements functions such as intensity control, operating point control, and light attenuation control, but the intensity modulator is an optical path through device. In contrast, MCSL is a reflective device. Although its intensity control mechanism is similar to that of the MC intensity modulator, it can simultaneously achieve reflection intensity and transmitted light emphasis control in a specific optical path application environment. For example, the MCSL as a fiber laser external cavity reflector, can achieve Q-switched laser or achieve output light intensity control, so it has special application

advantages. Moreover, the functional device also has further performance optimization space, for example, utilizing the large evanescent field characteristics of the MC and integrating it with a two-dimensional material such as graphene, which is expected to achieve a higher modulation rate [19].

4. Conclusion

In order to meet the development requirements of compact tunable fiber lasers, sensing and communication systems, it is important to develop new compact, low-cost, high-efficiency all-optical tunable filters and intensity modulators. This paper analyzes and investigates the MCSL's all-optical modulation characteristics caused by thermo-optical effects. According to the experimental results, by injecting pump lights with different intensities into the MCSL, tunable filters and intensity modulators based on MCSL can be achieved. The modulation efficiency is proportional to α , η , I_P and inversely proportional to r . The transmission spectra of MCSL shifts and the rate of wavelength shift is 1 pm/mW. In addition, at specific wavelength (e.g., 1550 nm), intensity modulation of MCSL can be achieved, and the amplitude of the modulation response signal increases linearly with the amplitude of pump light. And the modulation efficiency is directly proportional to the modulation frequency. The amplitude response characteristics of MCSL under intensity modulation are in accordance with that of the MC. In addition, the MCSL can be used as a reflectivity-tunable Sagnac reflector and this reflector can achieve the reflectivity variation of about 10% when the pump light is at milliwatt level. The research results show that MCSL can achieve the function of all-optical tunable filtering and is expected to realize the capability of broadband and multi-band tunable filtering if the structural parameters are properly designed. The MCSL is expected to play an important role in the development of tunable, multi-wavelength, compact fiber lasers.

Acknowledgment

The authors would like to thank J. Zhang for the help with article writing.

References

- [1] J. Wang, H. Luo, Z. Meng, and Y. Hu, "Experimental research of an all-polarization-maintaining optical fiber vector hydrophone," *J. Lightw. Technol.*, vol. 30, no. 8, pp. 1178–1184, Apr. 2012.
- [2] A. D. Ludlow, M. M. Boyd, J. Ye, E. Peik, and P. O. Schmidt, "Optical atomic clocks," *Rev. Mod. Phys.*, vol. 87, no. 2, pp. 637–701, 2014.
- [3] Z. Sun, A. Martinez, and F. Wang, "Optical modulators with 2D layered materials," *Nature Photon.*, vol. 10, pp. 227–238, 2016.
- [4] C. Ma *et al.*, "Integrated silicon photonic transmitter for polarization-encoded quantum key distribution," *Optica*, vol. 3, no. 11, pp. 1274–1278, 2016.
- [5] P. Sibson *et al.*, "Chip-based quantum key distribution," *Nature Commun.*, vol. 8, 2017, Art. no. 13984.
- [6] P. Sibson, J. E. Kennard, S. Stanisic, C. Erven, J. L. O'Brien, and M. G. Thompson, "Integrated silicon photonics for high-speed quantum key distribution," *Optica*, vol. 4, no. 2, pp. 172–177, 2017.
- [7] X. Liu, X. Yang, F. Lu, J. Ng, X. Zhou, and C. Lu, "Stable and uniform dual-wavelength erbium-doped fiber laser based on fiber Bragg gratings and photonic crystal fiber," *Opt. Exp.*, vol. 13, no. 1, pp. 142–147, 2005.
- [8] R. A. Pérez-Herrera, L. Rodríguez-Cobo, M. A. Quintela, J. L. Higuera, and M. López-Amo, "Single-longitudinal-mode dual wavelength switchable fiber laser based on superposed fiber Bragg gratings," *IEEE Photon. J.*, vol. 7, no. 2, 2015, Art. no. 7101307.
- [9] T. Zhai *et al.*, "Dual-wavelength polymer laser based on an active/inactive/active sandwich-like structure," *Appl. Phys. Lett.*, vol. 109, no. 10, pp. 1833–1295, 2016.
- [10] T. Zhu *et al.*, "Tunable dual-wavelength fiber laser with ultra-narrow linewidth based on Rayleigh backscattering," *Opt. Exp.*, vol. 24, no. 2, pp. 1324–1330, 2016.
- [11] S. Li, R. Li, L. Li, R. Liu, L. Gao, and X. Chen, "Dual wavelength semiconductor laser based on reconstruction-equivalent-chirp technique," *IEEE Photon. Technol. Lett.*, vol. 25, no. 3, pp. 299–302, Feb. 2013.
- [12] X. M. Liu, "Broad and tunable multiwavelength fiber laser at the assistance of modulation-instability-assisted four-wave mixing," *Laser Phys.*, vol. 20, no. 4, pp. 842–846, 2010.
- [13] H. B. Sun, X. M. Liu, Y. K. Gong, X. H. Li, and L. R. Wang, "Broadly tunable dual-wavelength erbium-doped ring fiber laser based on a high birefringence fiber loop mirror," *Laser Phys.*, vol. 20, no. 2, pp. 522–527, 2010.
- [14] R. H. Stolen, Chinlon Lin, and R. K. Jain, "A time-dispersion-tuned fiber Raman oscillator," *Appl. Phys. Lett.*, vol. 30, no. 7, pp. 340–342, 2008.

- [15] Y. Zhou, K. K. Y. Cheung, S. Yang, P. C. Chui, and K. K. Y. Wong, "A time-dispersion-tuned picosecond fiber-optical parametric oscillator," *IEEE Photon. Technol. Lett.*, vol. 21, no. 17, pp. 1223–1225, Sep. 2009.
- [16] X. Liu *et al.*, "Tunable and switchable multi-wavelength erbium-doped fiber laser with highly nonlinear photonic crystal fiber and polarization controllers," *Laser Phys. Lett.*, vol. 5, no. 12, pp. 904–907, 2008.
- [17] X. Liu *et al.*, "Versatile multi-wavelength ultrafast fiber laser mode-locked by carbon nanotubes," *Sci. Rep.*, vol. 3, no. 9, 2013, Art. no. 2718.
- [18] P. Wang *et al.*, "Packaged optical add-drop filter based on an optical microfiber coupler and a microsphere," *IEEE Photon. Technol. Lett.*, vol. 28, no. 20, pp. 2277–2280, Oct. 2016.
- [19] J. Chen, B. Zheng, G. Shao, S. Ge, F. Xu, and Y. Lu, "An all-optical modulator based on a stereo graphene–microfiber structure," *Light: Sci. Appl.*, vol. 4, no. 12, 2015, Art. no. e360.
- [20] L. Chao, P. Liy, W. Liangying, W. Yiqun, W. Sijun, and Y. Shaowei, "Analysis of all fiber acousto-optic tunable filter based on superimposed fiber Bragg gratings," *Acta Physica Sinica*, vol. 64, no. 17, 2015, Art. no. 174207.
- [21] J. Jie, F. Xuanqi, Z. Yao, Q. Xinyuan, H. Qingli, and B. Jintao, "Tunable dual-wavelength filter based on cascaded acousto-optic gratings in diam-etched fiber," *Acta Photonica Sinica*, vol. 44, no. 8, 2015, Art. no. 0806005.
- [22] W. Danning, W. Yuanda, W. Yue, A. Junming, and H. Xiongwei, "Research on tunable filter based on micro-ring resonators," *Acta Photonica Sinica*, vol. 36, no. 1, 2016, Art. no. 0123002.
- [23] F. Wei *et al.*, "Magnetic field sensor based on a combination of a microfiber coupler covered with magnetic fluid and a Sagnac loop," *Sci. Rep.*, vol. 7, no. 1, 2017, Art. no. 4725.
- [24] Y. Chen, Y. Semenova, G. Farrell, F. Xu, and Y.-Q. Lu, "A compact Sagnac loop based on a microfiber coupler for twist sensing," *IEEE Photon. Technol. Lett.*, vol. 27, no. 24, pp. 2579–2582, Dec. 2015.
- [25] S. Pu, L. Mao, T. Yao, J. Gu, M. Lahoubi, and X. Zeng, "Microfiber coupling structures for magnetic field sensing with enhanced sensitivity," *IEEE Sensors J.*, vol. 17, no. 18, pp. 5857–5861, Sep. 2017.
- [26] S. Pu, L. Luo, J. Tang, L. Mao, and X. Zeng, "Ultrasensitive refractive-index sensors based on tapered fiber coupler with Sagnac loop," *IEEE Photon. Technol. Lett.*, vol. 28, no. 10, pp. 1073–1076, May 2016.
- [27] L. Sun *et al.*, "Investigation of humidity and temperature response of a silica gel coated microfiber coupler," *IEEE Photon. J.*, vol. 8, no. 6, Dec. 2016, Art. no. 6805410.
- [28] M. Ding, P. Wang, and G. Brambilla, "A microfiber coupler tip thermometer," *Opt. Exp.*, vol. 20, no. 5, pp. 5402–5408, 2012.
- [29] H. Ahmad and A. A. Jasim, "Fabrication and characterization of 2×2 microfiber coupler for generating two output stable multiwavelength fiber lasers," *J. Lightw. Technol.*, vol. 35, no. 19, pp. 4227–4233, Oct. 2017.
- [30] J. Chen *et al.*, "Microfiber-coupler-assisted control of wavelength tuning for Q-switched fiber laser with few-layer molybdenum disulfide nanoplates," *Opt. Lett.*, vol. 40, no. 15, pp. 3576–3579, 2015.
- [31] Y. Yu, B. Qiang, N. Zhang, Y. Lu, X. Zhang, and J. Yang, "Investigation on an all-optical intensity modulator based on an optical microfiber coupler," *Chin. Opt. Lett.*, vol. 16, no. 4, 2018, Art. no. 040605.
- [32] Y. Yu, Q. Bian, K. Guo, X. Zhang, and J. Yang, "Experimental investigation on the characteristics of all-optical modulation of optical microfiber coupler," *IEEE Photon. J.*, vol. 10, no. 4, Aug. 2018, Art. no. 7103610.